

**Pedestrian evacuation simulation in the presence of an obstacle using self-propelled spherocylinders**I. Echeverría-Huarte , I. Zuriguel , and R. C. Hidalgo *Departamento de Física, Facultad de Ciencias, Universidad de Navarra, E-31080 Pamplona, Spain*

(Received 11 April 2020; accepted 15 June 2020; published 24 July 2020)

We explore the role that the obstacle position plays in the evacuation time of agents when leaving a room. To this end, we simulate a system of nonsymmetric spherocylinders that have a prescribed desired velocity and angular orientation. In this way, we reproduce the nonmonotonous dependence of the pedestrian flow rate on the obstacle distance to the door. For short distances, the obstacle delays the evacuation because the exit size is effectively reduced; i.e., the distance between the obstacle and the wall is smaller than the door width. By increasing the obstacle distance to the door, clogging is reduced leading to an optimal obstacle position (maximum flow rate) in agreement with results reported in numerical simulations of pedestrian evacuations and granular flows. For further locations, however, a counterintuitive behavior occurs as the flow rate values fall again below the one corresponding to the case without obstacle. Analyzing the head-times distribution, we evidence that this new feature is not linked to the formation of clogs, but is caused by a reduction of the efficiency of the agent's instantaneous flow rate when the exit is not blocked.

DOI: [10.1103/PhysRevE.102.012907](https://doi.org/10.1103/PhysRevE.102.012907)**I. INTRODUCTION**

The study of crowd evacuations in risky situations is a relevant task with a potential impact on society. Indeed, better knowledge of human collective behavior in these extreme circumstances should constitute the foundation of our efforts to build safer infrastructures and prevent a repeat of past tragedies [1–3]. The theoretical investigation of this topic started with the pioneering work of Helbing *et al.* [4], who performed simulations of evacuations in which the pedestrians were modeled as circular particles. Specifically, the pedestrian flow rate  $J$  was analyzed in enclosures with different geometries. Among all the parameters of the model investigated, the most important turned out to be the pedestrians' desired velocity, which in a congested scenario corresponds to the force that pedestrians exert on the people in front. In the bottleneck geometry, the variation of this parameter gave rise to the so called faster-is-slower (FIS) effect, which explains why adopting a more competitive behavior in a crowd can produce a delay in the global evacuation time. In addition, in that work it was also proposed that if an obstacle is placed on the upstream side of the exit, the flow rate can be enhanced because it would alleviate the pressure at the door and consequently reduce the development of clogging events.

Since that first numerical approach to pedestrian dynamics, many other models have been developed (see [5] for a recent review). Among them, the most widely used are cellular automata, lattice-gas, discrete element, and fluid dynamics models. In general, the outcomes reported are positive about Helbing's suggestions. Most of them reproduce the FIS phenomenon [6–8], and they agree that locating an obstacle in front of the door may improve the evacuation times [7,9–11]. Escobar and De La Rosa [12] studied the effect of different architectural configurations (including the obstacle) on the flow rate in an evacuation process using the social force model. Their findings evidenced that the obstacle caused an

overall reduction in particle velocities and an improvement in the outflow. However, the positive results were limited as they depended on the number of particles used: with more than 100 pedestrians, the obstacle ceased to be efficient. Kirchner *et al.* [13] also evidenced the convenience of placing an obstacle in evacuations, but the approach was different as they used a cellular automata model in which the role of friction between pedestrians was proven to be crucial. Furthermore, Hughes [9] discusses the suitability of placing barriers for flow improvement from a macroscopic point of view. In addition, other aspects related to the obstacle are studied, such as its shape [14], its position with respect to the exit [7,15], or its distribution [16,17]. In all of them (see [18] for a recent review) it is concluded that the presence of the obstacle does not always lead to an evacuation improvement.

In parallel to the development of numerical models, several experiments with human participants have been implemented to investigate room evacuation [19–22]. Among them, some authors have tested the possible beneficial role of the obstacle. In [10] a small group of participants was asked to exit through an 82 cm door with a 42 cm cabinet placed in front. The results reported a 30% improvement in the flow over the no-obstacle case. Yanagisawa *et al.* [23] also reported beneficial effects of placing a 20 cm column in front of a 50 cm door (a 7% improvement in the flow rate). After that, Liu *et al.* [24] and Shi *et al.* [25] conducted a series of controlled experiments in which different architectural settings for the obstacle and the exit were examined. In both cases, it was found that locating the exit door in a corner (instead of in the wall center) was an optimal strategy for increasing the flow rate; however, using an obstacle could be inefficient as it can increase the egress time.

Importantly, it should be remarked that the evacuating conditions in these experimental drills were only weakly competitive, in the sense that pushing each other was not allowed and contacts were only occasional. More recently,

Garcimartín *et al.* [26,27] have moved forward and performed controlled experiments in which participants were allowed to push moderately and the emerging pressure in the crowd was important. They tested different evacuating conditions implementing several kinds of obstacles and positions. Unexpectedly, no improvement was seen in the evacuation times, challenging the current paradigm that placing an obstacle before the exit can be beneficial for crowd evacuation.

Finally, let us note that some other experiments about the role of an obstacle in bottleneck flows have been carried out with animals such as ants [28], sheep [29], and mice [30]. Generally speaking, these works concluded that the obstacle could be beneficial on certain occasions but its position has to be carefully chosen. Importantly, it should be remarked that although these animal analogies can be inspiring and useful to understand some generic features of pedestrian bottleneck flow, it is important to avoid setting direct comparisons with human behavior.

Given all this, it is not surprising that understanding the actual role of the obstacle in a room evacuation is one of the most controversial topics in the field of pedestrian dynamics [31]. In this respect, it is reasonable to make two observations. The first observation is that one should not assume an obstacle is always beneficial for crowd evacuation [18]. The second concerns the limitations of Helbing's model in reproducing human behavior under highly competitive conditions. An additional purely geometric degree of complexity emerges in a real system when the agents are asymmetric. Indeed, body orientation has recently attracted the attention of the pedestrian dynamics community [32–34], and it seems that in very dense conditions the shape of the agents could become even more determinant [35]. Therefore, our work tries to fill this gap, implementing a model with noncircular pedestrians to explore the evacuation process in the presence of an obstacle. Note that taking into account the rotational motion of a nonspherical body not only gives a better description of the problem, but it also opens the possibility of analyzing the effect of new variables that would not exist if we worked with circular particles. One such variable is the pedestrian desired body orientation with respect to the displacement direction, a parameter that was introduced in [36,37] and will also be investigated in this paper.

Our model simulates a set of spherocylindrical bodies flowing through a bottleneck in different competitive conditions, some of which lead to high densities and contact forces among the particles. In our study, we evaluate the effectiveness of placing an obstacle in front of the door by measuring the flow rate and the distributions of time lapses between consecutive outgoing pedestrians, also known as head-times. Fixing the door and obstacle sizes, we carry out a systematic study, exploring the effect of three parameters of our model: the desired speed of the particles, the distance from the obstacle to the door, and the rotational strength (that determines the force with which each pedestrian tries to keep its desired orientation).

Our work is organized as follows: Section II exposes the numerical model and the explored situations. Section III describes the outcomes and their discussion for each set of parameters. Finally, we present the main conclusions of this work and suggest different future lines of research.

## II. NUMERICAL SIMULATION

### A. The model

The numerical model used in this work is based on discrete element method modeling, and it was already introduced in [36]. Here, we will summarize its main features and carefully describe an important modification that has been incorporated in the bodies' noise in order to make them more realistic. As in previous works, the bodies' shape is approximated by a spherocylinder, so they can be characterized by their short and long axis. Here, the values taken for these variables are distributed in the range of 0.35–0.5 m for the long axis and 0.24–0.33 m for the short axis. The mass of each body is distributed as a truncated normal distribution in the range 45–114 kg. The choice of these numbers is based on the actual size and weight of the people that performed the evacuation drills reported in [38].

In our approach, the particle motion is driven by a self-propulsion mechanism, while a granular-type force accounts for the local particle-particle interactions. The self-propulsion force can be thought of as an energy input provided by each individual particle, and it reads

$$\vec{F}_{Di} = m_i \frac{(\vec{v}_i - \vec{V}_d)}{\tau}, \quad (1)$$

where  $\vec{v}_i$  and  $\vec{V}_d = V_d \cdot \hat{e}_i$  are the velocity of the particle and the desired velocity, respectively. The direction of the vector  $\hat{e}_i$  fixes the desired direction to the target place, which is defined as the closest point of the door. In practice, the target is generally chosen as a segment located at the exit line, the length of which is slightly shorter (16%) than the door size. Finally,  $\tau$  is a characteristic time interpreted as the time that the pedestrian would take to reach the speed  $V_d$  in the case of free movement (no interaction with other bodies). Its value is set to  $\tau = 0.5$  s, as is commonly used in the literature [4,10].

In addition, the contact force  $\vec{F}_{Gi}$  has two terms,

$$\vec{F}_{Gi} = \sum_j^{N_c} \vec{F}_{ij} + \vec{F}_{wi}, \quad (2)$$

where  $\vec{F}_{wi}$  is the interaction between the particle and the walls, and the sum accounts for all the forces  $\vec{F}_{ij}$  between particle  $i$  and its  $N_c$  contacting neighbors.

Importantly, the action of each interparticle force  $\vec{F}_{ij}$  produces a torque  $\vec{r}_{ij} \times \vec{F}_{ij}$  on the particle. Thus, the total granular torque reads

$$\tau_{Gi} = \sum_j^{N_c} \vec{r}_{ij} \times \vec{F}_{ij}, \quad (3)$$

where  $r_{ij}$  is the branch vector drawn from the center of mass of  $i$  to the contact point with particle  $j$ .

Our numerical scheme also includes a self-alignment torque  $\Gamma_{Di}$ , which mimics the desire of pedestrians to walk with their shoulder plane aligned perpendicularly to the direction of movement. In practice, the torque is set proportional to  $\Delta\theta$ , the difference among the actual and the desired orientation of the particle [36,37]. The complete expression of the

self-alignment torque reads

$$\Gamma_{Di} = [S_D \Delta \theta - \beta \dot{\theta} + \eta] \cdot \hat{z}. \quad (4)$$

Note that the first term of the equation is an elastic term characterized by an angular strength  $S_D$ . It also contains a linear damping term  $\beta \dot{\theta}$ , where  $\theta$  is the particle's angular velocity. In the simulation, we set  $\beta = 4.5\sqrt{S_D}$ , which guarantees overdamped conditions.

The self-alignment torque [Eq. (4)] also includes a white noise  $\eta$  that differs from the one introduced in previous works [36,37]. In that case, the noise remained active during the whole evacuation process, having a deterministic and periodic nature that does not seem to represent people's behavior during an evacuation in a realistic manner. Indeed, previous experiments showed that people who are far from the door typically keep their body oriented toward the exit. Once they approach the door, the possibility of getting trapped in a given configuration increases, and pedestrians try to rotate their bodies to escape from it. In other cases, intentional body rotations are performed to occupy some existing gaps within the crowd, and it seems that this strategy is more frequent near the exit. For this reason, we consider that introducing a continuous perturbation in the particle rotation is not a proper way of modeling human behavior. Therefore, we propose an implementation of the noise that is only activated if the pedestrian is close to the door and is not moving. In practice, the noise is introduced at each particle when it fulfills two conditions: (i) it is closer to the center of the door than 2.2 m, and (ii) its kinetic energy is below an energy threshold (five orders of magnitude lower than the initial energy of the particle).

Importantly, the strength of the noise  $\eta$  is chosen from a normal distribution  $\eta \sim \mathcal{N}(0, \sigma_\eta)$ , with  $\sigma_\eta = 170$  N m. This value was taken after estimating the typical torque acting on a clogged pedestrian. To this end, we performed preliminary simulations without any noise; in this scenario, whenever a clog developed, the torques acting on each particle that configured the blocking arch were sampled. Repeating the simulations as many times as necessary, we drew the global distribution of torques involved, resulting in a Gaussian with  $\mu_\eta \approx 0$  and  $\sigma_\eta \approx 170$  N m.

Once the forces and torques are defined, the translational and rotational dynamics of each particle are resolved using velocity Verlet schemes. As stated above, more details about the numerical implementation can be found in [36,37].

### B. Simulated scenarios

We simulate 192 agents within a square room of  $8 \times 8$  m<sup>2</sup> flowing continuously through a door of 1.0 m width placed in the middle of one wall. This door size is sufficiently large to prevent a complete arrest of the flow and small enough to trigger partial flow interruptions. Initially, all pedestrians are distributed throughout the room with random speeds (translational and rotational), and their angular position is fixed in  $\pi$  radians (all facing the wall where the door is). We used periodic boundary conditions to avoid transient effects. In practice, this implies that all pedestrians passing through the door at a given position in the  $x$  direction (coordinates indicated in Fig. 2) reenter the room from the back at the same

$x$  position. For practical reasons, we also applied periodic boundary conditions in the transversal direction, but we have checked that for the size of the room and the number of pedestrians simulated here, there are no pedestrians reaching these boundaries. Furthermore, in some tests a circular obstacle of 1 m radius is implemented (results for smaller obstacle sizes are shown in the Appendix). The obstacle is always placed with its center aligned with the center of the door, and we vary systematically its distance to the exit in the  $y$  direction. This is quantified by the parameter  $\Delta$ , which specifically accounts for the distance from the center of the door to the closest part of the obstacle, as indicated in Fig. 2(b).

All the results presented here were obtained setting a simulation time of  $T_{\text{sim}} \sim 1500$  s. This time guarantees that all particles leave the room at least five times during the simulation. In addition, in order to have good statistics, several repetitions of the simulations with the same parameter values were also executed but varying the initial conditions (rotational and translational particle speeds). Indeed, it is important to note that depending on the parameter values, the number of repetitions performed was different. As we will see later, when the value of the desired velocity is high, the variability of the results is notably larger. That is why, in those specific cases, it was necessary to increase the number of repetitions in order to reduce the uncertainty of the measured magnitudes.

We execute a systematic study, varying the desired speed  $V_d$ , the angular strength  $S_D$ , and the distance of the obstacle to the door  $\Delta$ . Modifying  $V_d$ , we aim to reproduce changes in the competitiveness level, while the parameter  $S_D$  allows us to vary the tendency of the particles to align in a specific direction. A value of  $S_D$  close to zero makes the particle rotational motion unconstrained, so the particle does not have a desired orientation in its movement toward the door. On the contrary, when  $S_D$  is higher than zero, the particle tends to orient its long axis perpendicular to the direction of the desired velocity. The higher  $S_D$  is, the stronger is the force that the body applies to reduce the difference between its actual orientation and its desired orientation. Lastly, introducing the obstacle and modifying its position, we investigate the role it plays on the pedestrian evacuation process.

Our systematic study begins by evaluating the dependence of the flow rate on the desired velocity  $V_d$  for cases without an obstacle (NO) and no desired orientation ( $S_D = 0$ ). This scenario serves as a reference to compare when exploring the significance of the other parameters investigated. Then, we will introduce the obstacle, keeping the angular strength null and varying the parameter  $\Delta$  (obstacle distance to the door) to find out whether there are positions that optimize the flow. As a last step, we modify the strength of orientation  $S_D$ , addressing its influence on the flow properties.

## III. RESULTS

### A. Evacuation without obstacle and no desired orientation

We start by evaluating the system response when varying the desired speed  $V_d$  for evacuations without an obstacle and  $S_D = 0$ . In every run, we obtained the exit time for each pedestrian, which is then used to calculate the head-times  $\tau$  between the passage of consecutive individuals. This variable is ideal to detect the formation of blockages at the exit, and

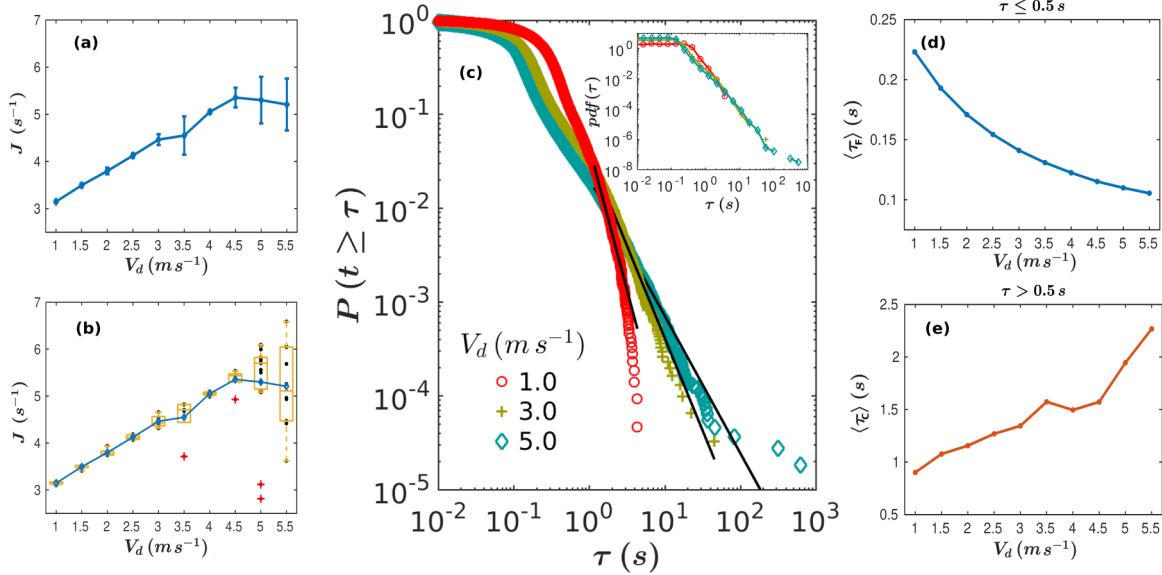


FIG. 1. (a) Average flow rates (calculated as the mean of the different repetitions performed in the same conditions) vs pedestrian desired speed  $V_d$ . Error bars have been calculated as the standard error with a confidence level of 95%. (b) Black dots represent the average flows obtained for each repetition (lasting 1500 s), and blue dots represent the means of these data, which correspond to same values displayed in (a). Also, the box plots of the data are shown in yellow: the boxes display the median and the interquartile range (IQR), and the whiskers reach the closest data point inside 1.5 IQR. Those points that remain outside this range are represented as outliers (red crosses). (c) Complementary cumulative distribution function of the time intervals ( $\tau$ ) between the passage of two consecutive pedestrians for different  $V_d$  values as indicated in the legend. Solid lines represent power-law fittings of the tails with the exponent values reported in Table I. Inset: log-log representation of the probability density functions for the same simulations as in the main panel. In (d) and (e) we show the time interval averages when considering only the time lapses that are smaller or larger than a preestablished threshold ( $\tau_c = 0.5$ ). This separates the clogging and flowing condition:  $\tau_c$  for  $\tau \leq 0.5$  and  $\tau_f$  for  $\tau > 0.5$ .

it can also be used to compute other magnitudes such as the flow rate as  $J = 1/\langle \tau \rangle$ . Once the value of  $J$  is calculated for each repetition (1500 s), we obtain the average value for each type of evacuation condition. Figure 1(a) suggests a nonmonotonous dependency of  $J$  on the desired velocity  $V_d$ . For low values of  $V_d$ , the flow rate increases with  $V_d$  denoting a *faster-is-faster* regime. However, the behavior changes at  $V_d \simeq 4.5$  m s<sup>-1</sup> as  $J$  saturates and even seems to decrease slightly when increasing  $V_d$ , hence suggesting a *faster-is-slower* effect.

Nonetheless, increasing  $V_d$  also produces more dispersion in the measurements, as can be glimpsed from the error bars of Fig. 1(a). These error bars have been calculated as the 95% confidence intervals of all repetitions performed in the same conditions. To confirm this result, in Fig. 1(b) we represent the whole statistics by means of box-plots (also, black dots are used to represent the values of  $J$  calculated in each repetition). The results displayed in Fig. 1(b) confirm an important increase of dispersion in the flow rate values when  $V_d$  augments, a feature that is especially evidenced by the presence of outliers (red crosses). Therefore, although the data seem to display a *faster-is-slower* behavior for high values of  $V_d$ , the high dispersion in the values of  $J$  obtained in these conditions demands a better and more careful analysis of the individual passage times  $\tau$  (recall that  $J$  can be understood as just the inverse of the average of the head-times  $J = 1/\langle \tau \rangle$ ).

As expected, the probability distributions of head-times are strongly asymmetric [inset of Fig. 1(c)]. They display a plateau for low passage times and then—after a certain

value of  $\tau$  that we will call  $\tau_{\min}$ —a decay that is compatible with the power-law tail already obtained in other systems such as grains, colloids, and sheep [39]. Aiming at a better quantification of these heavy tails (which reflect the existence of long-lasting clogs), in Fig. 1(c) we show the complementary cumulated distribution functions  $P(t \geq \tau)$  (also called survival functions). First, we confirm the existence of power-law decays,  $p(\tau) \sim t^{-\alpha}$ . Moreover, a fitting of the curves reveals that all tails have exponents  $\alpha > 2$  (see Table I), so the first moment of the distribution  $\langle \tau \rangle$  is well defined. This is relevant as it implies that the values of  $J$  represented in Fig. 1(a) are also well defined.

Having said that, it is also important to remark that, in some cases, the values of  $\alpha$  are below 3; when this happens, the second moment of the distribution diverges. In practice, this means that the standard deviation of these distributions cannot be univocally defined: it will grow unboundedly as the measuring time increases. This feature can of course be related to the high dispersion in the values of  $J$  reported in Fig. 1(b). Indeed, in this plot the outliers (represented with red crosses) always appear toward low values of  $J$  as they are caused by extreme long-lasting clog events.

Doing a more careful analysis of Fig. 1(c), it is noticeable that the survival functions show different trends depending on the values of  $\tau$  that we look at. For low values of  $\tau$ , the probability  $P(t \geq \tau)$  increases as the value of  $V_d$  decreases. Conversely, for high values of  $\tau$  (approximately from  $\tau > 1$  s) this trend is reversed. In this region, it is more probable to find long-lasting head-times when the value of  $V_d$  increases, a

TABLE I. Values of some parameters for different  $V_d$  values:  $\alpha$  is the exponent of the power-law tail,  $\tau_{\min}$  is the value of  $\tau$  above which the fit is valid,  $\langle\tau\rangle$  is the average evacuation time per pedestrian,  $s_\tau$  is the variance of  $\tau$  values, and  $N$  is the total number of data recorded. The \* signs in  $s_\tau$  indicate that the second moment of the distribution is not well defined as the exponent value is  $\alpha \leq 3$ . Indeed, in most of these cases the value of  $s_\tau$  is similar to or much larger than the value of  $\langle\tau\rangle$ .

| $V_d$ (m s <sup>-1</sup> ) | $\alpha$ | $\tau_{\min}$ (s) | $\langle\tau\rangle$ (s) | $s_\tau$ (s) | $N$    |
|----------------------------|----------|-------------------|--------------------------|--------------|--------|
| 1                          | 4.03     | 1.16              | 0.318                    | 0.103        | 21864  |
| 1.5                        | 3.73     | 1.50              | 0.286                    | 0.140        | 24081  |
| 2                          | 3.03     | 1.11              | 0.263                    | 0.166        | 26169  |
| 2.5                        | 2.86     | 1.09              | 0.242                    | 0.233*       | 28417  |
| 3                          | 2.97     | 1.38              | 0.224                    | 0.283*       | 30745  |
| 3.5                        | 2.86     | 1.50              | 0.220                    | 3.202*       | 31290  |
| 4                          | 2.84     | 1.45              | 0.198                    | 0.525*       | 34785  |
| 4.5                        | 2.62     | 1.27              | 0.187                    | 0.338*       | 36799  |
| 5                          | 2.46     | 1.16              | 0.189                    | 9.374*       | 109550 |
| 5.5                        | 2.34     | 1.01              | 0.192                    | 9.950*       | 71653  |

behavior that is compatible with the reduction of the exponent  $\alpha$  when increasing  $V_d$ , as reported in Table I. A similar behavior has been observed before in granular and sheep flow through bottlenecks [40], and it has been attributed to an increase of clogging. As in that work, in order to study both regions separately and characterize the different trends observed, we define a threshold of  $\tau_t = 0.5$  s, which determines if the system is in a *flowing condition* (if  $\tau \leq \tau_t$ ) or in a *clogged scenario* (when  $\tau > \tau_t$ ). Physically, this means assuming that a clog only happens when the delay among the passage of consecutive pedestrians is longer than 0.5 s; otherwise, the flow is continuous and the existence of small delays is just a consequence of the discrete nature of our system. Importantly, the same analysis that would be presented below was done using another threshold of  $\tau_t = 1.0$  s, obtaining very similar results.

Once the distinction among flowing and clogged conditions has been made, we calculate the average  $\tau$  values for each case (we called them  $\langle\tau_F\rangle$  and  $\langle\tau_C\rangle$ , respectively). The outcomes are reported in Figs. 1(d) and 1(e), revealing that, as the desired speed  $V_d$  increases,  $\langle\tau_F\rangle$  monotonically decreases and  $\langle\tau_C\rangle$  monotonically increases. In one, if the system is not clogged, pedestrians pass faster as the competitiveness increases. However, when the system is clogged, augmenting the competitiveness enlarges the duration of the exit blockages. In other words, our outcomes suggest that regardless of the desired velocity, there is a *faster-is-faster* behavior for events with  $\tau \leq \tau_t$ , and a *faster-is-slower* behavior for events with  $\tau > \tau_t$ . Thereby, the impact of the desired speed on the flow rate depends strongly on the state of the system. When the system is in fluidized conditions, increasing the desired speed would enhance the particle flow rate. However, when the system is stuck, increasing the desired speed would enlarge the duration of clogs, hence diminishing the global flow rate. These features suggest that the competition between the dynamics in these two regimes determines the overall system response. Note that this behavior can be masked by the simplistic calculation of the average flow rate; then, our result

stresses the importance of taking into account the statistical properties of the head-times distributions in order to have a complete picture of the evacuation dynamics (see [41,42] for a deeper explanation). Although it may be thought that the tails have little statistical weight, their role in the dynamics can be very significant. An example of this instance can be sensed by looking at the high value of  $\langle\tau_C\rangle$  obtained for  $V_d = 3.5$  m s<sup>-1</sup>, which is caused by a single very long-lasting clog, which also leads to an extraordinarily low value of  $J$  for the run in which it appeared [see the outlier in Fig. 1(b)].

## B. Effect of the obstacle

After investigating the role that the desired velocity plays in room evacuations, we proceed to examine the effect of placing an obstacle in front of the door. For this purpose, we perform new simulations implementing a circular obstacle of radius  $R = 1.0$  m, which is aligned with the center of the door. We have carried out a systematic study, varying the distance from the obstacle to the door  $\Delta$  for the same desired speeds  $V_d$  implemented in Sec. III A. Figure 2(a) illustrates the values of flow rate  $J = 1/\langle\tau\rangle$  as a function of  $\Delta$  for four representative values of  $V_d$ .

In general, we find that the qualitative dependence of  $J$  on  $\Delta$  is approximately the same regardless of the desired velocity. When the obstacle is placed very close to the door, the flow rate is notably lower than in the case without the obstacle [dotted lines in Fig. 2(a)]. The reason is that for these obstacle positions, pedestrians get stuck as the area between the wall and the obstacle narrows, as illustrated in Fig. 2(b). In this scenario, the door size plays a secondary role and the characteristic size governing the system dynamics is the width of these narrow passages at both sides of the obstacle. As the obstacle is separated from the door, the size of these lateral passages increases, and the flow rate is enhanced until an optimal distance is reached (around 1.2 m). Then, as the obstacle distance to the door is further increased, the flow rate reduces and tends to the asymptotic limit of the case without an obstacle. Interestingly, this asymptotic approximation to the no-obstacle scenario seems to depend on the desired velocity. For the lowest value ( $V_d = 1$  m s<sup>-1</sup>), the flow rate after the optimum obstacle position is always higher than that in the case without an obstacle. Therefore, there is a gradual approach to the asymptotic limit from above, a result that is compatible with the one obtained experimentally for clogging in granular materials [43]. Nevertheless, for the other desired velocities displayed in Fig. 2(a), the flow rate drops below the dotted line when  $\Delta > 1.5$  m, so the obstacle delays the evacuation before approaching the asymptotic limit from below. As far as we know, this distinctive feature has not been reported experimentally in any system of discrete bodies passing through bottlenecks. In the same way, we are not aware of any numerical work that has reported this kind of behavior.

Aiming to rationalize the different trends observed when changing the place of the obstacle, we analyze the survival functions of the time-lapses in the same way as before. In Fig. 3 we display the outcomes obtained for several obstacle positions and three representative values of the desired velocity. The first salient feature is that the distributions display the

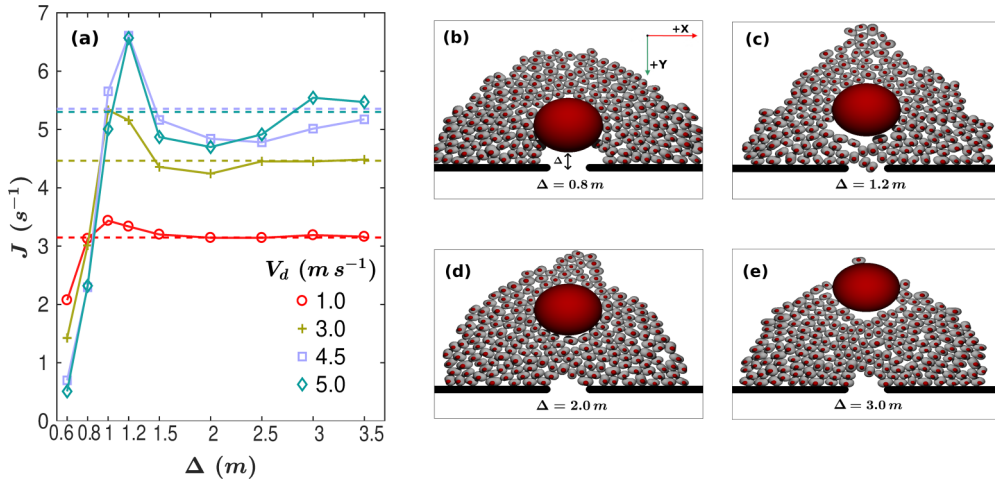


FIG. 2. Effect of obstacle position on the flow rate. (a) Average flow rates vs obstacle position, for several values of desired speed  $V_d$  as indicated in the legend. Dotted lines represent the asymptotic limit, which corresponds to the case without obstacle. (b)–(e) Snapshots of the simulations obtained for different obstacle positions as indicated in each panel.

same characteristic power-law tails as those obtained without an obstacle [reported in Fig. 1(a)]. Interestingly, for the lowest velocity analyzed, all distributions are very similar, a behavior that is compatible with the small dependence of the flow rate on the obstacle position reported in Fig. 2 for this case. On the contrary, for higher desired velocities, the exponent  $\alpha$  seems to depend nonmonotonically on the obstacle distance to the door  $\Delta$ . Effectively, when the obstacle is too close to the door, the distribution tails are the heaviest, and for the specific case of  $\Delta = 0.6 m$  they approach the limit  $\alpha = 2$ , where  $\langle \tau \rangle$  is not well-defined. Remarkably, the survival functions also capture the optimal position of the obstacle at  $\Delta = 1.2 m$ . In this case, the statistics show the lowest probabilities of long head times, a hallmark of clogging reduction. Conversely, when  $\Delta > 2.0 m$  we are unable to detect any feature in the distributions that correlates with the local minimum in the flow rate reported in Fig. 2 for these obstacle positions.

To attain a better quantification of the different flowing dynamics emerging in the presence of an obstacle, we follow the same procedure as before and we analyze separately the passage statistics when the system is in a *flowing condition* ( $\tau \leq \tau_f$ ) and when it is *clogged* ( $\tau > \tau_f$ ). Again, we use  $\tau_f = 0.5 s$  as a threshold value to recalculate the average head-time for each regime separately. Figure 4 shows the obtained dependencies of  $\langle \tau_f \rangle$  and  $\langle \tau_c \rangle$  on  $\Delta$  for different desired speeds  $V_d$ . Interestingly, Fig. 4(a) reveals that when the system is in the *flowing condition*, the obstacle never reduces the pedestrian passage times (at least in a significant manner). This occurs regardless of the desired velocity of the pedestrians and the position of the obstacle. However, when the system is clogged [Fig. 4(b)], the presence of the obstacle at certain distances improves the flow as  $\langle \tau_c \rangle$  are sometimes lower than in the case without an obstacle. Indeed, we observe that the lowest value of  $\langle \tau_c \rangle$  occurs for  $\Delta$  around

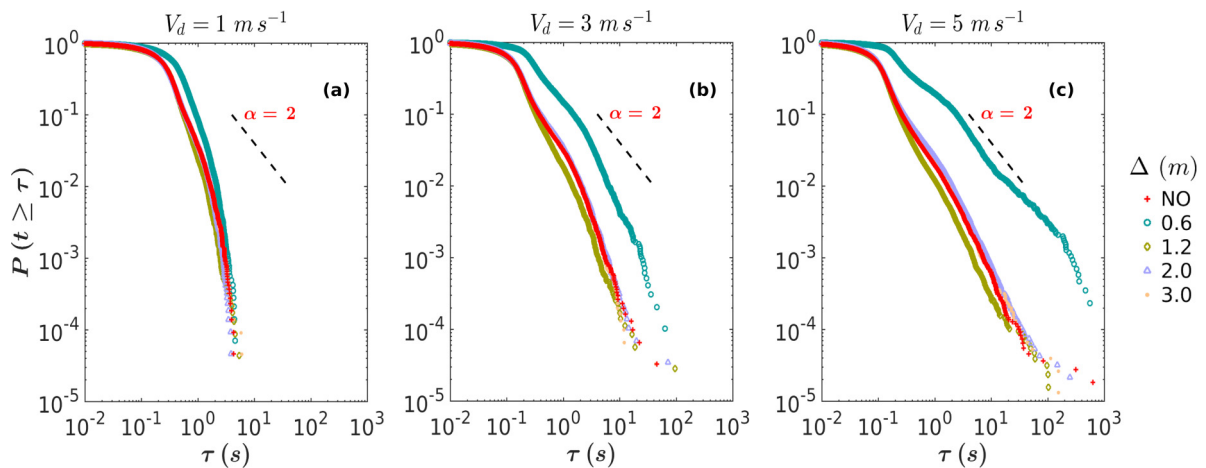


FIG. 3. Complementary CDFs of the time lapses obtained for different  $V_d$  values and obstacle positions (see the legend, where NO means absence of obstacle). In each panel, the results for all the simulations with the same  $V_d$  are represented: 1, 3, and 5  $m s^{-1}$  for (a)–(c), respectively, as indicated at the top of each panel. The black dotted line marks the boundary  $\alpha = 2$  below which the expected average value of the distribution does not converge.

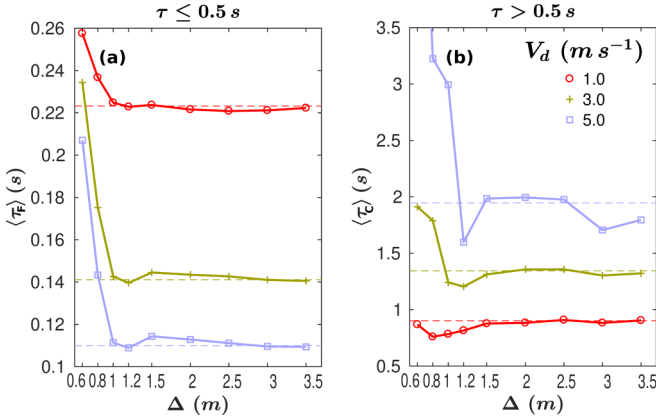


FIG. 4. Average head times as a function of the obstacle distance for different values of the desired velocity (see the legend). In (a) the average  $\langle\tau_F\rangle$  is performed over the values of  $\tau$  when the system is flowing (i.e.,  $\tau < 0.5$ ), whereas in (b) the average  $\langle\tau_C\rangle$  is performed when the system is clogged (i.e.,  $\tau > 0.5$ ). The colored dotted lines indicate the asymptotic limit for the no-obstacle case.

1.2 m, coinciding with the obstacle position at which the maximum flow rate appeared in Fig. 2. Overall, this behavior indicates that the obstacle effect on reducing clogging times is the reason that it improves the flow rate for some specific positions (as suggested in the original paper of Helbing *et al.* [4]). Nevertheless, the existence of a local minimum in the flow rate for  $\Delta > 1.5$  m cannot be explained by the obstacle effect on clogging.

Interestingly, a closer analysis of the average head-times in the *flowing condition* [Fig. 4(a)] reveals a small but systematic increase of  $\langle\tau_F\rangle$  for  $\Delta > 1.5$  m that leads to a local maximum around  $\Delta = 2$  m. Therefore, it seems that the presence of the obstacle at these distances negatively affects the instantaneous flow rate (the flow rate value when there are no blockages). Accordingly, we can conclude that the existence of a local minimum on the flow rate reported in Fig. 2 for  $\Delta \simeq 1.5$  is related to the dynamics emerging in the flowing condition. A different way of reaching this conclusion is observing that  $\langle\tau_F\rangle$  approaches the no-obstacle limit from above, a behavior compatible with the flow rate behavior displayed in Fig. 2(a) (where the asymptotic limit was reached from below). Again, as happened in that case, the behavior observed for  $V_d = 1 \text{ m s}^{-1}$  seems to be the exception to the rule, as  $\langle\tau_F\rangle$  approaches the no-obstacle limit from below.

After all, the actual macroscopic system response results from a competition between the dynamics in the flowing and clogged condition. In spite of the fact that the system is flowing most of the time, it seems that the blockages (being extreme in some cases) are the ones that primarily determine the flow rate of the system. In this way, thanks to the positive role that the obstacle plays in avoiding the formation of long-lasting clogs, the flow rate is notably enhanced for obstacle positions around 1.2 m. Then, when the obstacle is placed at further distances ( $\Delta > 1.5$  m), this clogging prevention effect is reduced and the seemingly negative role that the obstacle has on the instantaneous flow leads to the appearance of a local minimum on the flow rate.

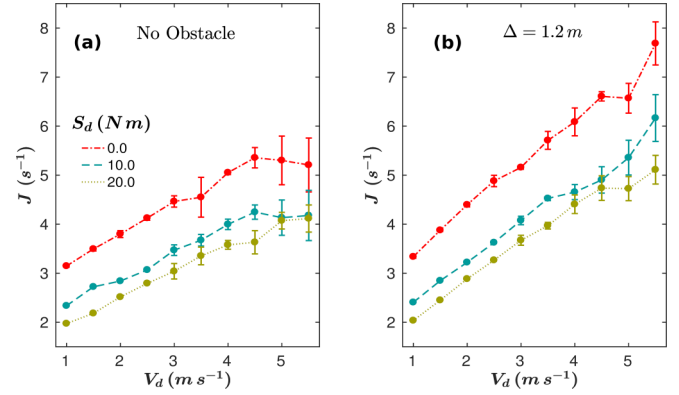


FIG. 5. Average flow rates vs pedestrian desired speed  $V_d$  for three different values of  $S_D$  (0, 10, 20 N m). As representative cases, we display results for the simulations without obstacle (a) and with the obstacle placed at  $\Delta = 1.2$  m (b). All error bars have been calculated as the 95% confidence interval of the average of all runs computed in the same conditions.

### C. Influence of angular strength $S_D$

As a last step, we analyze the influence of the parameter  $S_D$  on the pedestrian flow. Until this point, we set the value of  $S_D = 0 \text{ N m}$ , so the particles had no preferred angular orientation. By increasing the value of  $S_D$ , we force the bodies to reduce the difference between their current and desired orientation (long axis perpendicular to the desired velocity direction) by applying a torque such as that defined in Eq. (4). This investigation is performed considering the case without an obstacle and the scenario where the obstacle position optimizes the flow rate ( $\Delta = 1.2$  m). Furthermore, we test three different values of angular strength ( $S_D = 0, 10, 20 \text{ N m}$ ) for the whole range of desired velocities explored in previous sections.

In Fig. 5(a) the outcomes of the flow rate  $J$  are presented as a function of the desired velocity for the case without an obstacle. Clearly, the best scenario is when particles propel without any preferred orientation ( $S_D = 0$ ) and the flow rates reduce when increasing  $S_D$ . Comparatively, the greatest change is seen when increasing the value of  $S_D$  from 0 to 10 N m, with a smaller effect if we keep augmenting  $S_D$  up to 20 N m. More importantly, it seems that the implementation of the angular strength screens the appearance of the faster-is-flower effect for high values of the desired velocity.

In the presence of the obstacle [Fig. 5(b)], the evolution of the flow rate curves is rather similar to the case without an obstacle. Again, increasing  $S_D$  leads to smaller flow rates and masks the appearance of the FIS effect. Indeed, the obstacle seems to prevent the emergence of FIS even for the evacuations for particles with no desired orientation [blue curves in Fig. 5(b)], a feature that is compatible with the reduction of the clogging events triggered by the obstacle that was evidenced before.

We proceed now to display in Fig. 6 the dependence of the survival functions on the angular strength for four representative cases (with and without an obstacle and low and high desired velocity). Clearly, the most important parameter affecting the distributions tails is the desired velocity. As is known, increasing  $V_d$  augments the probability of finding long

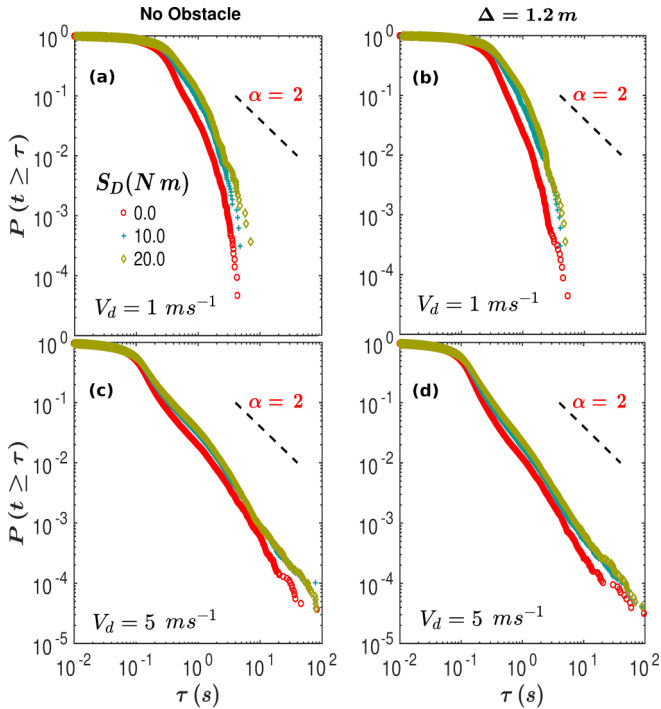


FIG. 6. Complementary cumulative distribution functions of the time lapses obtained for  $V_d = 1 \text{ m s}^{-1}$  (top row) and  $V_d = 5 \text{ m s}^{-1}$  (bottom row) when there is no obstacle (left panels) and when the obstacle is placed at  $\Delta = 1.2 \text{ m}$  (right panels). Different colors are used for distinct values of  $S_D$  as indicated in the legend. Again, the black dotted lines mark the boundary  $\alpha = 2$  after which the average value of the distribution does not converge.

arrests of the flow. In addition, we find a weak (but consistent) effect of the angular strength on the appearance of these long clogs: when  $S_D > 0$ , the tails seem to be a little bit wider than for the case of  $S_D = 0$ . This behavior, which happens regardless of whether or not the obstacle is present, is coherent with the flow rate reduction reported in Fig. 5 when increasing  $S_D$ .

To test this hypothesis, we will compute once again the average head-time when the system is in the flowing condition or in the clogged one. Interestingly, the dependence of the obtained values on the desired velocity reported in Fig. 7 is very similar regardless of whether or not there is an obstacle: when  $V_d$  increases,  $\langle \tau_F \rangle$  reduces and  $\langle \tau_C \rangle$  augments, both monotonically. As expected from the trends reported in the distribution tails in Fig. 6, the effect of implementing an angular strength slightly increases  $\langle \tau_C \rangle$  [note that red and yellow curves are systematically above the blue ones in panels (c) and (d)]. But surprisingly, the effect of  $S_D$  on the system dynamics is more apparent when focusing on the flowing condition [Figs. 7(a) and 7(b)]. Clearly, implementing a preferred orientation in the evacuating pedestrians affects the instantaneous flow (when there are no clogs), which becomes lower ( $\langle \tau_F \rangle$  higher) as  $S_D$  is increased.

Overall, the results reported in this section suggest that implementing an angular strength—which seems a suitable strategy if we want to simulate a more realistic pedestrian behavior—delays the evacuation process. Contrary to what it could be *a priori*, forcing a prescribed body orientation has only a reduced effect on the clog formation and duration, and

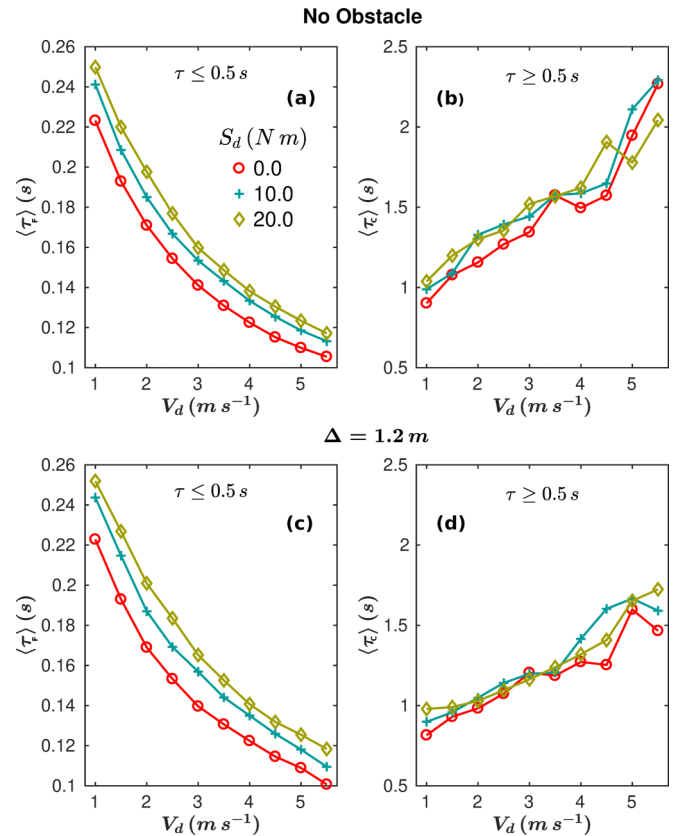


FIG. 7. Average head times as a function of the desired velocity when measured in either the flowing condition ( $\langle \tau_F \rangle$ , top panels) or in the clogged scenario ( $\langle \tau_C \rangle$ , bottom panels). As in the previous figure, results are presented when there is no obstacle (left panels) and when the obstacle is placed at the optimal position  $\Delta = 1.2 \text{ m}$  (right panels). The different curves in each figure correspond to distinct values of  $S_D$  as indicated in the legend.

a more important impact on the dynamics when the system is freely flowing. Although the origin of this behavior is not clear, we speculate that it could be driven by a reduction of the global ordering near the door when the bodies are aligned with the shoulders perpendicular to the desired velocity direction. On the contrary, the emergence and duration of the clogs would be mostly determined by the intensity of the  $\eta$  noise that was introduced above in Eq. (4). Note that this noise is not coupled to the value of  $S_D$ , and therefore it seems quite reasonable that the clogging statistics are rather similar for the three cases of  $S_D$  presented.

#### IV. CONCLUSION

In this work, we have simulated the flow of self-propelled asymmetric spherocylinders through a narrow door as an approximation to the pedestrian room evacuation problem. To this end, we have used a previously introduced model [36] in which we incorporated a new and more realistic noise in those pedestrians that are stacked at the exit proximities. In this way, we have performed a systematic investigation of the flow rate dependence on several parameters of the model: desired velocity  $V_d$ , obstacle distance to the door  $\Delta$ , and angular strength  $S_D$ . By determining the time gaps between

the passage of consecutive pedestrians, we have been able to characterize the bottleneck flow process, which evidences the existence of two different dynamics: when the crowd is *flowing* and when it is *clogged*.

The study of these two dynamics separately has allowed us to consistently reveal the faster-is-slower effect in the clogged condition and the faster-is-faster phenomenon in the flowing one. This happens regardless of the desired velocity values analyzed, the obstacle placement, and the angular strength implemented. Consequently, we can state that the prevalence and competition between these two regimes is what determines the overall emergence of the faster-is-slower effect. For example, when the obstacle is introduced—although the faster-is-slower effect appears in the clogging condition—clogs are importantly reduced and their weight in the statistics is not sufficiently important to cause the appearance of the faster-is-slower effect in the average flow rate.

In this sense, we have also shown that the reduction of clogging induced by the obstacle is clearly behind the existence of an optimal distance at which the flow rate is globally improved. On the contrary, the presence of a local minimum in the flow rate when the obstacle is at about 2 m seems to be caused by a negative effect of the obstacle in the system dynamics when it is in a flowing condition. Finally, we observe that the torque inducing pedestrians to align their bodies perpendicularly to the moving direction is, in all cases, prejudicial for the flow rate developed. This stresses the importance of implementing more realistic particle shapes to develop better and more helpful evacuation models.

There are several points that we leave open for future work. First of all, it would be important to meticulously characterize the micromechanics of the system, thus allowing us to obtain density, speed, and force fields in different conditions. In addition, it would be interesting to break the symmetry of the room, offsetting the obstacle from the exit door. This task would of course be very challenging as it will imply the addition of a new degree of freedom in the system, and the performance of a whole set of numerical experiments varying that parameter (but also the other ones). Nevertheless, we believe it is a promising and worthwhile approach given the experimental evidence existing about the efficacy of this strategy [23].

#### ACKNOWLEDGMENTS

This work was funded by Ministerio de Economía y Competitividad (Spanish Government) through Project No.

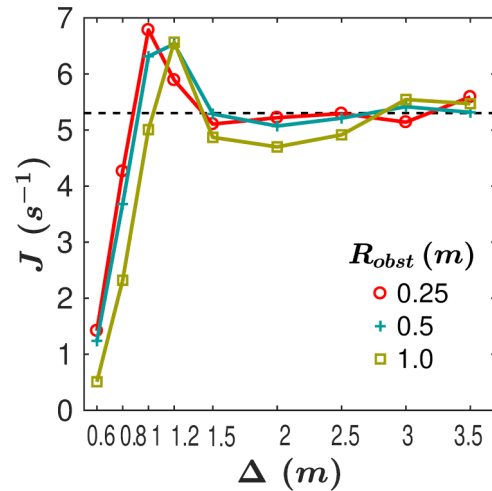


FIG. 8. Average flow rate for pedestrians moving with a desired velocity  $V_d = 5 \text{ m s}^{-1}$  as a function of the obstacle position. Different colors correspond to different obstacle radius as indicated in the legend. The dotted line represents the asymptotic limit, which corresponds to the case without obstacle.

FIS2017-84631-P, MINECO/AEI/FEDER, UE. I.E. acknowledges Asociación de Amigos de la Universidad de Navarra for his grant.

#### APPENDIX: EFFECT OF OBSTACLE SIZE

In this Appendix, we analyze the role that the obstacle size has on the macroscopic flow rate. To this end, apart from the obstacle implemented in the paper, we have simulated two smaller sizes of 0.5 and 0.25 m radius. Interestingly, the results reported in Fig. 8 for the most interesting case of  $V_d = 5 \text{ m s}^{-1}$  reveal that the flow rate improvement is similar regardless of the obstacle size. Nevertheless, the optimum obstacle position seems to move toward smaller values of  $\Delta$ , a behavior that seems reasonable as, for a given obstacle location, reducing the obstacle size implies enlarging the narrow passages at both sides of the obstacle. Also, the comparison among different obstacle sizes suggests that the decrease of flow appearing for  $\Delta \simeq 2.0 \text{ m}$  is minimized when the obstacle size is reduced. In any case, a further investigation of the role of obstacle size and shape would be interesting using nonsymmetric spherocylinders.

- 
- [1] J. B. Thomas and C. Peters, *Int. J. Retail Distrib. Manage.* **39**, 522 (2011).
  - [2] R. F. Fahy, G. Proulx, and L. Aiman, *Fire Matter* **36**, 328 (2012).
  - [3] K. Rogers, *Women's Stud. Quart.* **40**, 171 (2012).
  - [4] D. Helbing, I. Farkas, and T. Vicsek, *Nature (London)* **144**, 297 (2000).
  - [5] H. Vermuyten, J. Beliën, L. De Boeck, G. Reniers, and T. Wauters, *Safety Sci.* **57**, 167 (2016).
  - [6] D. R. Parisi and C. O. Dorso, *Physica A* **385**, 343 (2007).
  - [7] G. A. Frank and C. O. Dorso, *Physica A* **390**, 2135 (2011).
  - [8] K. Suzuno, A. Tomoeda and D. Ueyama, *Phys. Rev. E* **88**, 052813 (2013).
  - [9] R. Hughes, *Annu. Rev. Fluid Mech.* **35**, 169 (2003).
  - [10] D. Helbing, L. Buzna, A. Johansson, and T. Werner, *Transport. Sci.* **39**, 1 (2005).
  - [11] Y. Zhao, M. Li, X. Lu, L. Tian, Z. Yu, K. Huang, Y. Wang, and T. Li, *Physica A* **465**, 175 (2017).

- [12] R. Escobar and A. De La Rosa, *Lect. Notes Comput. Sci.* **2801**, 97 (2003).
- [13] A. Kirchner, K. Nishinari, and A. Schadschneider, *Phys. Rev. E* **67**, 056122 (2003).
- [14] D. Helbing and A. Johansson, in *Encyclopedia of Complexity and Systems Science*, edited by R. Meyers (Springer, New York, 2010).
- [15] T. Matsuoka, A. Tomoeda, M. Iwamoto, K. Suzuno, and D. Ueyama, *Traffic and Granular Flow'13* (Springer, Cham, 2015).
- [16] N. Shiwakoti and M. Sarvi, *Transport. Res. Pt. C* **37**, 260 (2013).
- [17] L. Jiang, J. Li, C. Shen, S. Yang, and Z. Han, *PLoS ONE* **9**, e115463 (2014).
- [18] N. Shiwakoti, X. Shi, and Z. Ye, *Safety Sci.* **113**, 54 (2019).
- [19] S. Hoogendoorn and W. Daamen, *Transport. Sci.* **39**, 147 (2005).
- [20] A. Seyfried, O. Passon, B. Steffen, M. Boltes, T. Rupprecht, and W. Klingsch, *Transport. Sci.* **43**, 395 (2009).
- [21] C. Feliciani and K. Nishinari, *Transp. Res. Pt. C* **91**, 124 (2018).
- [22] T. Kretz, A. Grünebohm, and M. Schreckenberg, *J. Stat. Mech.* (2016) P10014.
- [23] D. Yanagisawa, A. Kimura, A. Tomoeda, R. Nishi, Y. Suma, K. Ohtsuka, and K. Nishinari, *Phys. Rev. E* **80**, 036110 (2009).
- [24] Y. Liu, X. Shi, Z. Ye, N. Shiwakoti, and J. Lin, in *Proceedings of the 16th COTA International Conference of Transportation Professionals: CICTP 2016* (ASCE, Reston, VA, 2016), pp. 779–790.
- [25] X. Shi, Z. Ye, N. Shiwakoti, D. Tang, and J. Lin, *Physica A* **522**, 350 (2019).
- [26] A. Garcimartín, D. Maza, J. M. Pastor, D. R. Parisi, C. Martín-Gómez, and I. Zuriguel, *New J. Phys.* **20**, 123025 (2018).
- [27] I. Zuriguel, I. Echeverría, D. Maza, R. C. Hidalgo, C. Martín-Gómez, and A. Garcimartín, *Safety Sci.* **121**, 394 (2020).
- [28] N. Shiwakoti, M. Sarvi, G. Rose, and M. Burd, *Transport. Res. Record* **2137**, 31 (2009).
- [29] I. Zuriguel, J. Olivares, J. M. Pastor, C. Martín-Gómez, L. M. Ferrer, J. J. Ramos, and A. Garcimartín, *Phys. Rev. E* **94**, 032302 (2016).
- [30] P. Lin, J. Ma, T. Y. Liu, T. Ran, Y. L. Si, F. Y. Wu, and G. Y. Wang, *Physica A* **482**, 227 (2017).
- [31] M. Haghani, *Safety Sci.* **129**, 104760 (2020).
- [32] C. Feliciani and K. Nishinari, in *Proceedings of Pedestrian and Evacuation Dynamics 2016, Collective Dynamics* (2016), p. 76.
- [33] J. H. Yamamoto, D. Yanagisawa, C. Feliciani, and K. Nishinari, *Transport. Res. Pt. B* **122**, 486 (2019).
- [34] J. Willems, A. Corbetta, V. Menkovski, and F. Toschi, *arXiv:2001.04646*.
- [35] F. Alonso-Marroquin, J. Busch, C. Chiew, C. Lozano, and Á. Ramírez-Gómez, *Phys. Rev. E* **90**, 063305 (2014).
- [36] R. C. Hidalgo, D. R. Parisi, and I. Zuriguel, *Phys. Rev. E* **95**, 042319 (2017).
- [37] D. R. Parisi, R. Cruz Hidalgo, and I. Zuriguel, *Sci. Rep.* **8**, 1 (2018).
- [38] A. Garcimartín, J. M. Pastor, C. Martín-Gómez, D. Parisi, and I. Zuriguel, *Sci. Rep.* **7**, 1 (2017).
- [39] I. Zuriguel, D. R. Parisi, R. C. Hidalgo, C. Lozano, A. Janda, P. A. Gago, J. P. Peralta, L. M. Ferrer, L. A. Pugnaloni, E. Clément, D. Maza, I. Pagonabarraga, and A. Garcimartín, *Sci. Rep.* **4**, 7324 (2015).
- [40] J. M. Pastor, A. Garcimartín, P. A. Gago, J. P. Peralta, C. Martín-Gómez, L. M. Ferrer, D. Maza, D. R. Parisi, L. A. Pugnaloni, and I. Zuriguel, *Phys. Rev. E* **92**, 062817 (2015).
- [41] A. Nicolas, in *Traffic and Granular Flow 17*, edited by S. H. Hamdar (Springer International Publishing, Cham, 2019), pp. 357–364.
- [42] A. Nicolas, S. Bouzat, and M. N. Kuperman, *Transport. Res. Pt. B* **99**, 30 (2017).
- [43] I. Zuriguel, A. Janda, A. Garcimartín, C. Lozano, R. Arévalo, and D. Maza, *Phys. Rev. Lett.* **107**, 278001 (2011).